Received: 10 July 2020 | Revised: 7 May 2021 | Accepted: 10 May 2021

DOI: 10.1002/mma.7571

RESEARCH ARTICLE

WILEY

Mathematical modeling of tumor surface growth with necrotic kernels

Hua Zhang[1] | **Jianjun Paul Tian**[2] | **Ben Niu**[3] | **Yuxiao Guo**[3]

[1]Department of Mathematics, Harbin Institute of Technology, Harbin, Heilongjiang, China

[2]Department of Mathematical Sciences, New Mexico State University, Las Cruces, New Mexico, USA

[3]Department of Mathematics, Harbin Institute of Technology, Weihai, Shandong, China

Correspondence
Ben Niu, Department of Mathematics, Harbin Institute of Technology, Weihai, Shandong 264209, China.
Email: niu@hit.edu.cn

Communicated by: B. Niu

Funding information
National Institutes of Health, Grant/Award Number: U54CA132383; National Science Foundation of US, Grant/Award Number: DMS-1446139; Foundation for Innovation at HIT (WH)

A two-dimensional tumor-immune model with the time delay of the adaptive immune response is considered in this paper. The model is designed to account for the interaction between cytotoxic T lymphocytes (CTLs) and cancer cells on the surface of a solid tumor. The model considers the surface growth as a major growth pattern of solid tumors in order to describe the existence of necrotic kernels. The qualitative analysis shows that the immune-free equilibrium is unstable, and the behavior of positive equilibrium is closely related to the ratio of the immune killing rate to tumor volume growth rate. The positive equilibrium is locally asymptotically stable when the ratio is smaller than a critical value. Otherwise, the occurrence of the delay-driven Hopf bifurcation at the positive equilibrium is proved. Applying the center manifold reduction and normal form method, we obtain explicit formulas to determine the properties of the Hopf bifurcation. The global continuation of a local Hopf bifurcation is investigated based on the coincidence degree theory. The results reveal that the time of the adaptive immune system taken to response to tumors can lead to oscillation dynamics. We also carry out detailed numerical analysis for parameters and numerical simulations to illustrate our qualitative analysis. Numerically, we find that shorter immune response time can lead to longer patient survival time, and the period and amplitude of a stable periodic solution increase with the increasing immune response time. When CTLs recruitment rate and death rate vary, we show how the ratio of the immune killing rate to tumor volume growth rate and the first bifurcation value change numerically, which yields further insights to the tumor-immune dynamics.

KEYWORDS

global continuation, Hopf bifurcation, stability, surface contact, tumor-immune model

MSC CLASSIFICATION

37G15; 34K40

1 | INTRODUCTION

Cancer, an unnatural growth phenomenon of cell numbers, remains mostly an intractable disease despite the fact that tremendous advances have been made in treatment techniques and medicine.[1,2] Finding effective strategies for tumor

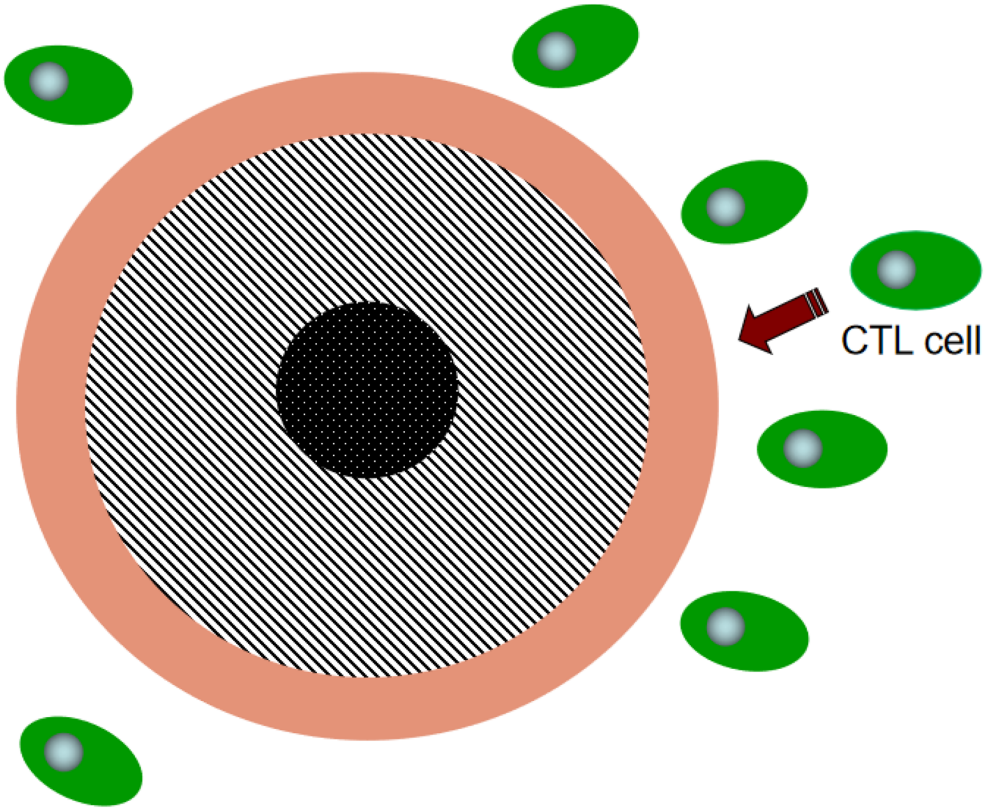

FIGURE 1 A tumor with a necrotic kernel and surface tumor-immune interaction [Colour figure can be viewed at wileyonlinelibrary.com]

control and therapies is significant for public health, as well as for economic resources. However, it is a great challenge since the growth and control of tumors involve a considerable number of biological mechanisms and dynamical processes that are too complicated to be fully captured. As studies of complexities in physics, tumor-associated responses can be better approached by establishing mathematical models with some appropriate simplified assumptions than via experimental procedures alone.[3–6]

Over the last two decades, tumor immunology has attracted remarkable attention and various mathematical models have been developed to understand the interaction between cancer and immune cells. A review of early works concerning tumor-immune interactions can be found in Adam and Bellomo[7] and Eftimie et al.[8] Given the complexity of this process, many models include four or more variables or equations. For example, Kuznetsov et al[9] proposed a system with five equations to investigate the mediated response to growing tumor mass, which can be applied to the tumor dormancy. However, in order to better recognise the main response mechanism between immune cells and tumor mass, some simplifications are excepted. Frascoli et al[10] presented a coupled ordinary equation system to account for the role of cytotoxic T lymphocytes (CTLs) in the growth of solid tumors, where CTLs can recognize and kill the cancer cells in a tumor and recruit other immune cells to the tumor site.[11] The structure of a tumor in Frascoli et al[10] was supposed to be a sphere with an inner shell representing a necrotic kernel, and the active cellular division only occurred on the surface of the tumor sphere; see Figure 1. A similar idea was also proposed in Kansal et al.[12]

There are two immune systems that can defend against cancer cells: the innate immune system as the first line of defence can lead to fast immune response. Macrophages and natural killer cells are two central types of innate immune cells in detecting and killing cancer cells. The adaptive immune response is slower to develop but manifests as antigenic specificity and memory increase. It consists of antibodies, B cells, and CD4+ and CD8+ T lymphocytes. Natural killer T cells and $\gamma\delta$ T cells are cytotoxic lymphocytes that straddle the interface of innate and adaptive immunity.[13] There might be a delay between the moment the cancer cells appear and the adaptive immune system is activated to work on cancer cells. CTLs belong to the adaptive immune system. To appropriately model CTLs-mediated immune response to tumor cells, the time delay of the adaptive immune response should not be ignored. Besides, numerous results such as those of previous works[14–16] have demonstrated that time delays can produce rich dynamics in a system, such as the stability switches and periodic oscillations. Bi et al[14] considered three delays that, respectively, described tumor cells proliferation, effector cells growth, and the immune effector cells differentiation and studied the oscillation activity of tumor and immune cells.

Parameter	Description	Biological ranges and unit
T_m	maximum volume of the tumor	$0 - 4 \times 10^6$ μm^3
ρ	recruitment rate of CTLs	0 – 0.97 μm day^{-1}
r	growth rate of the tumor	0 – 0.5 μm day^{-1}
k	killing rate of CTLs for the tumor	0 – 2.42 μm day^{-1}
d	death rate of CTLs	0 – 0.5 day^{-1}

TABLE 1 Common ranges and units for parameters in system (2), estimated based on Frascoli et al[10]

A solid tumor grows from a slow avascular growth period due to the nutrient limitation. Interested by the CTLs-mediated immune response on this stage, Frascoli et al[10] proposed the following model:

$$\begin{cases} \dot{V}(t) = \rho r_t V^{2/3}(t) - \rho k V^{2/3}(t) C(t), \\ \dot{N}(t) = \rho r_c V^{2/3}(t) N(t) - d_c N(t). \end{cases} \tag{1}$$

Here, $V(t)$ and $N(t)$ stand for the volume of a tumor mass and the number of CTLs with the ability to attack tumor cells at time t, respectively. It is assumed that the tumor has a spherical shape and the radius changes when tumor grows, so the tumor surface area is proportional to $\rho V^{2/3}(t)$, where ρ is the dimensionless shape factor changing with the tumor volume. r_c is the CTLs' recruitment rate, and r_t is the growth rate of tumor volume. The death rate of CTLs is denoted by d_c, and the rate at which cancer cells are killed by CTLs is k. $C(t)$ is a dimensionless function that stands for the fraction of the attacked surface area. All parameters in system (1) are positive.

Note that the term $V^{2/3}(t)N(t)$ is a functional response with fractional powers. This type of response functions has been widely used (see previous studies[17–19] and references therein). Chattopadhyay et al[19] proposed that it was better to use surface area rather volume when modeling the prey in groups. They further verified that the fractional term significantly affected the existence of interior equilibrium and periodic solutions. Kaslik and Neamtu[17] presented stable oscillations induced by time delay and pointed out that small fractional orders was better for system to remain stable.

The logistic function is one common choice when modelling species growth. Thus, in this paper, we use it to describe the growth of tumor in the absence of CTLs. In addition, the Holling II response function is used to model tumor-CTLs interaction. It is more practical to use a discrete time delay to reflect the time for the adaptive immune system to respond to the tumor. Accordingly, we propose a two-compartment model as

$$\begin{cases} \frac{\mathrm{d}T(t)}{\mathrm{d}t} = rT^{2/3}(t)\left[1 - \frac{T(t)}{T_m}\right] - kT^{2/3}(t)\frac{N(t)}{N(t)+\beta}, \\ \frac{\mathrm{d}N(t)}{\mathrm{d}t} = \rho T^{2/3}(t-\tau)N(t-\tau) - dN^2(t), \end{cases} \tag{2}$$

where r is the growth rate of the tumor, T_m is the maximum volume of a tumor, d stands for the death rate of the CTLs, and ρ is the recruitment rate of CTLs. k is the killing rate of CTLs. Here, we assume the death of CTLs is nonlinear, the similar consideration can be found in Friedman et al.[20] All parameters are estimated based on Frascoli et al,[10] which are shown in Table 1, except that β is the half-saturation constant which is chosen as $0 - 0.6 \times 10^6$.

The main goal of this paper is to study the effect of adaptive immune response delay on the stability of system (2). In particular, we intend to seek some conditions such that system (2) undergoes a Hopf bifurcation at positive equilibrium. We are further going to analyze the properties of bifurcating periodic solutions in local and global ranges. In fact, the center manifold method and normal form theory presented by Hassard et al[21] and Faria[22] are two useful tools for this problem, and they have been applied by many literatures (see Adak and Bairagi[23] and Wei[24] and the references therein). Biologically, the Hopf bifurcation phenomenon implies that the tumor and CTLs interaction in a periodical fashion and the tumor mass can never be eradicated. It is also noticed that when the time required by CTLs to respond to the tumor is less than bifurcation value, the tumor and CTLs can be stable at the positive equilibrium. Moreover, following the global Hopf bifurcation theory given in Wu,[25] we verify the global continuation of the local Hopf bifurcation. Understanding how the parameters in model, especially the delay τ, affect the solutions is helpful for successful treatment.

The rest of this paper is organized as follows. In Section 2, we investigate the existence and stability of equilibria, establish the conditions for Hopf bifurcation, and obtain explicit formulas to determine the direction of the Hopf bifurcation and the stability of the periodic solutions. In Section 3, we discuss the global existence of the Hopf bifurcation. In Section 4, we carry out some numerical simulations to illustrate our analytical results and exhibit the effects of parameters in model on the bifurcation parameter. Finally, we give a brief conclusion in the last section.

The phase space for a two-dimensional functional differential equation is usually $C([-\tau, 0], \mathbb{R}^2)$. However, due to the fractional-order terms, system (2) is not well defined when $T(t) = 0$; thus, we consider system (2) on the space X throughout this paper, where

$$X = \{(T, N) \in C : C = C([-\tau, 0], \ Int(\mathbb{R}_+) \times \mathbb{R}_+)\},$$
$$\mathbb{R}_+ = \{y \in \mathbb{R} : y \geq 0\} \text{ and } Int(\mathbb{R}_+) = \{y \in \mathbb{R}_+ : y > 0\}.$$

From Hale and Lunel,[26] we see that for the initial value

$$0 < T(\theta), 0 < N(\theta), \theta \in [-\tau, 0],$$

there exists a maximum $t_m > 0$ such that (2) has a unique solution $(T(t), N(t))$ on $(0, t_m)$. We further claim that $0 < T(t) \leq T_m, 0 < N(t)$ for $t \in (0, t_m)$. Suppose that there exists $t_0 \in (0, t_m)$ such that $N(t_0) = 0$ and $N(t) > 0$ for $t \in (0, t_0)$. Then from the second equation of (2), we have

$$\dot{N}(t_0) = \rho x^2(t_0 - \tau)N(t_0 - \tau) > 0.$$

This is a contradiction, and then the positivity of $N(t)$ follows. From the positivity of $N(t)$ and the comparison principle of functional differential equation, we have $0 < T(t) \leq T_m$ for $t \in (0, t_m)$.

2 | BASIC ANALYSIS

In this section, we provide analysis on the local stability of equilibria and the existence of the Hopf bifurcation near the positive equilibrium. Moreover, the properties of the Hopf bifurcation are demonstrated.

2.1 | Local stability of boundary equilibria

Clearly, system (2) always has a boundary equilibrium $E_1 = (T_m, 0)$. Rescaling T by $T = x^3$, we have

$$\begin{cases} \dot{x}(t) = \dfrac{r}{3}\left[1 - \dfrac{x^3(t)}{T_m}\right] - \dfrac{k}{3}\dfrac{N(t)}{\beta + N(t)}, \\ \dot{N}(t) = \rho x^2(t - \tau)N(t - \tau) - dN^2(t). \end{cases} \tag{3}$$

Let $x(t) = T_m^{1/3}\hat{x}(t)$, $N(t) = \beta\hat{N}(t)$, $\hat{r} = rT_m^{-1/3}/3$, $\hat{k} = kT_m^{-1/3}/3$, $\hat{\rho} = \rho T_m^{2/3}$, $\hat{d} = d\beta$ and drop the hats; then system (3) becomes

$$\begin{cases} \dot{x}(t) = r[1 - x^3(t)] - \dfrac{kN(t)}{1 + N(t)}, \\ \dot{N}(t) = \rho x^2(t - \tau)N(t - \tau) - dN^2(t). \end{cases} \tag{4}$$

The boundary equilibrium $(T_m, 0)$ becomes $(1, 0)$. It is easy to get that the characteristic equation of the linearization associated with system (4) at $(1, 0)$ is

$$(\lambda + 3r)(\lambda - \rho e^{-\lambda\tau}) = 0. \tag{5}$$

Apparently, the stability of $(1, 0)$ depends on the roots of

$$\lambda - \rho e^{-\lambda\tau} = 0. \tag{6}$$

In the case of $\tau = 0$, $\lambda = \rho > 0$, which implies $(1, 0)$ is unstable. For $\tau > 0$, we can check that (6) has no zero root or purely imaginary roots. Thus, $(1, 0)$ remains unstable. Consequently, $(T_m, 0)$ is unstable. The result is concluded in the following theorem.

Theorem 2.1. *For system (2), the boundary equilibrium E_1 is unstable.*

Remark 2.1. Theorem 2.1 indicates that the immune-free equilibrium is unstable. Namely, once the adaptive immune system is activated, the volume of the tumor is no longer T_m but tends to some other states. In the following subsection, we will further discuss the long-time behavior of the volume of the tumor.

2.2 | Existence and local stability of positive equilibrium

We turn to the coexistence state of CTLs and tumor. Note that the possible positive equilibrium (T_*, N_*) of system (2) becomes $E_* = (x_*, N_*)$ of system (4) after the transformation above. Further, the system (4) has identical dynamics with the system (2) at E_*; thus, we only study system (4) in later discussions.

Some trivial calculations give the existence and uniqueness of positive equilibrium E_* as follows.

Lemma 2.1. *System (4) always has a unique positive equilibrium $E_* = (x_*, N_*)$, where $N_* = \rho x_*^2/d$ and x_* is the unique positive solution of $\rho x^5 + dx^3 - \rho\left(1 - \frac{k}{r}\right)x^2 - d = 0$.*

Proof. Assume that (x, N) is a positive solution for system (4). Then, the second equation of system (4) shows $N = \rho x^2/d$. Substituting it into the first equation, we have

$$\rho x^5 + dx^3 - \rho\left(1 - \frac{k}{r}\right)x^2 - d = 0. \tag{7}$$

Denote

$$H(x) = \rho x^5 + dx^3 - \rho\left(1 - \frac{k}{r}\right)x^2 - d. \tag{8}$$

Taking derivatives of both sides of Equation (8) with respect to x yields

$$H'(x) = 5\rho x^4 + 3dx^2 - 2\rho\left(1 - \frac{k}{r}\right)x. \tag{9}$$

Case I: If $1 - k/r \le 0$, then $H'(x) \ge 0$ for $x \ge 0$. Furthermore, $H(0) = -d < 0$, and $\lim_{x\to\infty} H(x) = \infty$. This implies that $H(x) = 0$ has a unique solution for $x \in (0, \infty)$;

Case II: If $1 - k/r > 0$, let $G(x) = 5\rho x^3 + 3dx - 2\rho\left(1 - \frac{k}{r}\right)$, then $H'(x) = xG(x)$. Since $G'(x) > 0$, $G(0) < 0$ and $\lim_{x\to\infty} G(x) = \infty$, there exists a unique $x_1 \in (0, \infty)$ such that $G(x_1) = 0$. Hence, $H'(x) < 0$ for $x \in (0, x_1)$; $H'(x) \ge 0$ when $x > x_1$. Notice that $H(x_1) < H(0) = -d < 0$ and $\lim_{x\to\infty} H(x) = \infty$. Thus, $H(x) = 0$ has a unique solution on (x_1, ∞). The proof is completed. □

Linearizing system (4) at E_* leads to

$$\begin{cases} \dot{x}(t) = -3rx_*^2 x(t) - \dfrac{kN(t)}{(1+N_*)^2}, \\ \dot{N}(t) = -2dN_* N(t) + 2\rho x_* N_* x(t-\tau) + \rho x_*^2 N(t-\tau). \end{cases} \tag{10}$$

The corresponding characteristic equation of (10) is

$$\lambda^2 + A\lambda + B + (C\lambda + D)e^{-\lambda\tau} = 0, \tag{11}$$

with $A = 2dN_* + 3rx_*^2$, $B = 6rdx_*^2 N_*$, $C = -\rho x_*^2$, $D = \frac{2\rho k x_* N_*}{(1+N_*)^2} - 3r\rho x_*^4$.

We show the stability of E_* when $\tau = 0$.

Theorem 2.2. *E_* is locally asymptotically stable for $\tau = 0$.*

Proof. When $\tau = 0$, (11) becomes

$$\lambda^2 + (A + C)\lambda + (B + D) = 0. \tag{12}$$

It can be easily verified that

$$A + C = (\rho + 3r)x_*^2 > 0,\ B + D = 3r\rho x_*^4 + \frac{2\rho k x_* N_*}{(1+N_*)^2} > 0.$$

It follows from the Routh–Hurwitz criterion that all characteristic roots of (12) have negative real parts. The proof is completed. □

For $\tau > 0$, let $i\omega(\omega > 0)$ be a root of (11); then we have

$$-\omega^2 + iA\omega + B + (iC\omega + D)e^{-i\omega\tau} = 0.$$

Separating the real and imaginary parts gives

$$\begin{aligned} D\cos\omega\tau + C\omega\sin\omega\tau &= \omega^2 - B,\\ D\sin\omega\tau - C\omega\cos\omega\tau &= A\omega. \end{aligned}$$

Adding the square of both sides of above two equations yields

$$\omega^4 + (A^2 - C^2 - 2B)\omega^2 + (B^2 - D^2) = 0,$$

and

$$\omega^2 = \frac{C^2 + 2B - A^2 \pm \sqrt{(A^2 - C^2 - 2B)^2 - 4(B^2 - D^2)}}{2}.$$

According to the expressions of A, B and C, we have

$$A^2 - C^2 - 2B = (2dN_* + 3rx_*^2)^2 - \rho^2 x_*^4 + 12rdx_*^2 N_* = 3\rho^2 x_*^4 + 9rx_*^4 > 0.$$

If

$$(H_1):\ B < D$$

is satisfied, then we obtain

$$\omega_0 = \frac{\sqrt{2}}{2}\sqrt{C^2 - A^2 + 2B + \sqrt{(C^2 - A^2 + 2B)^2 - 4(B^2 - D^2)}}. \tag{13}$$

Further, we have

$$\tau_j = \begin{cases} \dfrac{1}{\omega_0}\left[\arccos\dfrac{D(\omega_0^2 - B) - AC\omega_0^2}{C^2\omega_0^2 + D^2} + 2j\pi\right], & \cos\omega_0\tau > 0,\\ \dfrac{1}{\omega_0}\left[2\pi - \arccos\left(-\dfrac{D(\omega_0^2 - B) - AC\omega_0^2}{C^2\omega_0^2 + D^2}\right) + 2j\pi\right], & \cos\omega_0\tau < 0,\ j = 0, 1, 2, \ldots. \end{cases} \tag{14}$$

Let $\lambda = \alpha(\tau) + i\omega(\tau)$ be a root of (11) satisfying $\alpha(\tau_j) = 0$ and $\omega(\tau_j) = \omega_0$. Some calculations yield the following result.

Lemma 2.2. *If the assumption (H_1) holds, then* $\frac{\mathrm{d}\mathcal{R}e(\lambda(\tau))}{\mathrm{d}\tau}\Big|_{\tau=\tau_j} > 0$.

Proof. Differentiating both sides of (11) with respect to τ gives

$$\frac{\mathrm{d}\lambda(\tau)}{\mathrm{d}\tau} = \frac{(C\lambda + D)\lambda}{(2\lambda + A)e^{\lambda\tau} + C - (C\lambda + D)\tau}.$$

This leads to

$$\left[\frac{\mathrm{d}\mathcal{R}e(\lambda(\tau))}{\mathrm{d}\tau}\right]^{-1} = \mathcal{R}e\left[\frac{(2\lambda + A)e^{\lambda\tau} + C}{(C\lambda + D)\lambda} - \frac{\tau}{\lambda}\right].$$

Then we obtain

$$\left[\frac{\mathrm{d}\mathcal{R}e(\lambda(\tau))}{\mathrm{d}\tau}\right]^{-1}\Bigg|_{\tau=\tau_j} = \frac{D\omega_0(A\sin\omega_0\tau_j + 2\omega_0\cos\omega_0\tau_j) - C\omega_0^2(A\cos\omega_0\tau_j - 2\omega_0\cos\omega_0\tau_j + C)}{C^2\omega^4 + D^2\omega^2}$$
$$= \frac{A^2 - C^2 - 2B + 2\omega_0^2}{C^2\omega_0^2 + D^2}.$$

Again, using $A^2 - C^2 - 2B > 0$, we have $\frac{A^2-C^2-2B+2\omega_0^2}{C^2\omega_0^2+D^2} > 0$, which completes the proof. □

According to the results in Ruan and Wei,[27] we arrive at the following results.

Lemma 2.3. *For system (4), we have the following:*

(*i*) *If assumption* (H_1) *is not satisfied, then all roots of (11) have negative real parts for all* $\tau \geq 0$*;*
(*ii*) *If* (H_1) *holds, then there exists a sequence of values of* τ*:* $0 < \tau_0 < \tau_1 < \ldots < \tau_j < \ldots$ *such that all eigenvalues have negative real parts when* $\tau \in [0, \tau_0)$*; (11) has* $2(j+1)$ *roots with positive real parts when* $\tau \in (\tau_j, \tau_{j+1}], j = 0, 1, 2, \ldots$*; For* $\tau = \tau_j$*,* $j = 0, 1, 2, \ldots$*, (11) has exactly a pair of simple imaginary roots* $\pm i\omega_0$*.*

Now, based on the fundamental Hopf bifurcation theorem in Hale and Lunel,[26] we have the following stability results at E_* and the existence of Hopf bifurcations.

Theorem 2.3. *For system (4), the following results hold.*

(*i*) *Assume* (H_1) *is not satisfied; the positive equilibrium* E_* *is locally asymptotically stable for* $\tau \geq 0$*;*
(*ii*) *Assume* (H_1) *is satisfied; then* E_* *is locally asymptotically stable for* $\tau \in [0, \tau_0)$ *and unstable for* $\tau > \tau_0$*. Furthermore, a Hopf bifurcation takes place at* E_* *when* $\tau = \tau_j, j = 0, 1, 2, \ldots$.

Remark 2.2. Noticing that all results obtained above are closely related to (H_1), we a give brief discussion about it. Denote

$$\Gamma(x) = 9x(d + \rho x^2)^2 - 2\rho d\frac{k}{r}.$$

It can be verified that $\Gamma(x_*) > 0$ when $k/r \leq 1$. Note that $B - D = \frac{\rho r x_*^3}{(d+\rho x_*^2)^2}\Gamma(x_*)$; thus, $B > D$ always holds when $k/r \leq 1$. From the biological viewpoint, when the CTL killing rate is less than the tumor growth rate, the tumor is stable and cannot be easily influenced by some external factors. In a later study, we will give some numerical simulations to illustrate how other factors impact (H_1) and the existence of the Hopf bifurcation on the $k - r$ plane.

2.3 | Properties of the Hopf bifurcation

In the previous subsection, we have obtained a sufficient condition for the occurrence of the Hopf bifurcation. According to the center manifold theorem, we know that the projection of periodic solution bifurcating from the first bifurcation value τ_0 on the center manifold has the same stability with that of system (4). Therefore, we shall study the direction of the Hopf bifurcation and the stability of bifurcating periodic solutions with the center manifold theory and normal form method given in Hassard et al.[21] The details will be provided in Appendix A, and the consequence is stated as the following theorem.

Theorem 2.4. *Suppose that the assumption* (H_1) *is satisfied. In the neighborhood of* τ_j*,* $j = 0, 1, 2, \ldots$*, the Hopf bifurcation at* E_* *is forward (backward), and the periodic solutions bifurcating from* τ_0 *are orbitally asymptotically stable (unstable) if* $\mathcal{R}e(c_1(0)) < 0 (> 0)$.

The calculation of $c_1(0)$ is given in Appendix A; we shall carry out some numerical simulations to illustrate our theoretical analysis in Section 4.

3 | GLOBAL EXISTENCE OF PERIODIC SOLUTIONS

In this section, we always assume that (H_1) is satisfied and consider the global existence of the Hopf bifurcation at the point $(E_*, \tau_j), j = 0, 1, 2, \ldots$, by applying the global bifurcation result developed by Wu.[25]

Let $\mathcal{C} = C([-\tau, 0], Int(\mathbb{R}_+) \times \mathbb{R}_+)$ and $v_t = (x_t, N_t) \in \mathcal{C}$ with $v_t(\theta) = v(t+\theta)$ for $t \geq 0$, $\theta \in [-\tau, 0]$. System (4) can be abstracted as the following functional differential equation

$$\dot{v}(t) = F(v_t, \tau, s), \tag{15}$$

where

$$F(\Psi, \tau, s) = \begin{pmatrix} r(1-\psi_1^3(0)) - \frac{k\psi_2(0)}{1+\psi_2(0)} \\ \rho\psi_1^2(-\tau)\psi_2(-\tau) - d\psi_2^2(0) \end{pmatrix},$$

and $\Psi = (\psi_1, \psi_2) \in \mathcal{C}$. The mapping $F : \mathcal{C} \times \mathbb{R}_+^2 \to Int(\mathbb{R}_+) \times \mathbb{R}_+$ is completely continuous. To restrict F onto the subspace of $\mathcal{C}$ composed by all constant functions, we define the mapping $\hat{F} = F|_{Int(\mathbb{R}_+)\times\mathbb{R}_+^3} : Int(\mathbb{R}_+) \times \mathbb{R}_+^3 \to Int(\mathbb{R}_+) \times \mathbb{R}_+$. Obviously,

$$\hat{F}(v, \tau, s) = \begin{pmatrix} r(1-x^3) - \frac{kN}{1+N} \\ \rho x^2 N - dN^2 \end{pmatrix}. \tag{16}$$

Denote constant mapping $v_0 \in \mathcal{C}$ by v^*. The point $(v^*,\ \tau^*,\ s^*)$ is said to be a stationary solution of (15) if $\hat{F}(v^*, \tau^*, s^*) = 0$. Therefore, we get

(A1) $\hat{F} \in C^2(Int(\mathbb{R}_+) \times \mathbb{R}_+^3, Int(\mathbb{R}_+) \times \mathbb{R}_+)$.
Furthermore, under assumption (H_1), we have

$$\det(D_v\hat{F}(v, \tau, s)|_{v=v^*}) = \det\begin{pmatrix} -3x_*^2 & -\frac{k}{(1+N_*)^2} \\ 2\rho x_* N_* & \rho x_*^2 - 2dN_* \end{pmatrix} < 0.$$

Thus, we have

(A2) $D_v\hat{F}(v, \tau, s)$ at the positive equilibrium v^* is an isomorphism on $Int(\mathbb{R}_+) \times \mathbb{R}_+$.
It is also clearly that

(A3) $F(\Psi,\ \tau,\ s)$ is differentiable with respect to Ψ.
At any stationary solution $(v^*,\ \tau^*,\ s^*)$, the corresponding characteristic matrix is

$$\Delta(v^*, \tau^*, s^*)(\lambda) = \begin{pmatrix} \lambda + 3x_*^2 & \frac{k}{(1+N_*)^2} \\ -2\rho x_* N_* e^{-\lambda\tau} & \lambda - \rho x_*^2 e^{-\lambda\tau} + 2dN_* \end{pmatrix},$$

and then we obtain that

$$\det(\Delta(v^*, \tau^*, s^*)(\lambda)) = \lambda^2 + A\lambda + B + (C\lambda + D)e^{-\lambda\tau}, \tag{17}$$

where $A,\ B,\ C,\ D$ are defined as in (11).
The stationary solution $(v^*,\ \tau^*,\ s^*)$ is called a center if

$$\det\left(\Delta(v^*, \tau^*, s^*)\left(n\frac{2\pi i}{s}\right)\right) = 0$$

for some integer n. A center $(v^*,\ \tau^*,\ s^*)$ is said to be isolated if it is the only center in some neighborhood of $(v^*,\ \tau^*,\ s^*)$. It can be easily verified that $\left(v^*, \tau_j, \frac{2\pi}{\omega_0}\right), j = 0, 1, 2, \ldots$, are isolate centers based on the analysis in Section 2. We also know that there exist $\eta > 0, \xi > 0$ and a smooth curve $\lambda : (\tau_j - \eta, \tau_j + \eta) \to \mathbb{C}$ such that

$$\det\left(\Delta(v^*, \tau^*, s^*)(\lambda(\tau))\right) = 0,\ |\lambda(\tau) - i\omega_0| < \xi, \tag{18}$$

for all $\tau \in [\tau_j - \eta,\ \tau_j + \eta]$. Moreover, $\lambda(\tau_j) = i\omega_0$, $\frac{d\mathcal{R}e(\lambda(\tau))}{d\tau}\Big|_{\tau=\tau_j} > 0$. It can be proved that on $(\tau_j - \eta, \tau_j + \eta) \times \Omega_{\xi, \frac{2\pi}{\omega_0}}$,

(A4) $\det\left(\Delta(v^*, \tau^*, s^*)\left(u + i\frac{2\pi}{s}\right)\right) = 0$ if and only if $u = 0, \tau = \tau_j$ and $s = 2\pi/\omega_0$, $j = 0, 1, 2, \ldots$, where

$$\Omega_{\xi, \frac{2\pi}{\omega_0}} = \{(u, s) : 0 < u < \xi, |s - 2\pi/\omega_0| < \xi\}.$$

Define

$$\Sigma(F) = \mathrm{Cl}\{(v,\tau,s) \in \mathcal{C} \times \mathbb{R}_+^2 : v_{t+s} = u_t\},$$
$$N(F) = \{(v^*,\tau,s) \in Int(\mathbb{R}_+) \times \mathbb{R}_+^3 : F(v^*,\tau,s) = 0\},$$

and let $D\left(v^*, \tau_j, \frac{2\pi}{\omega_0}\right)$ be the connected component for the center $\left(v^*, \tau_j, \frac{2\pi}{\omega_0}\right)$ of (15) in $\Sigma(F)$.

Lemma 3.1. *$D\left(v^*, \tau_j, \frac{2\pi}{\omega_0}\right)$ is unbounded for each center $\left(v^*, \tau_j, \frac{2\pi}{\omega_0}\right)$.*

Proof. As in Wu,[25] we define

$$\mathcal{H}^{\pm}\left(v^*, \tau_j, \frac{2\pi}{\omega_0}\right)(u,s) = \det\left(\Delta\left(v^*, \tau_j \pm \eta, \frac{2\pi}{\omega_0}\right)\left(u + i\frac{2\pi}{s}\right)\right).$$

Assumption (A4) indicates that $\mathcal{H}^{\pm}\left(v^*, \tau_j, \frac{2\pi}{\omega_0}\right)(u,s) \neq 0$ for $(u,s) \in \Omega_{\xi,2\pi/\omega_0}$; then the first crossing number $\gamma\left(v^*, \tau_j, \frac{2\pi}{\omega_0}\right)$ is

$$\begin{aligned}\gamma\left(v^*, \tau_j, \frac{2\pi}{\omega_0}\right) &= \deg_B\left(\mathcal{H}^-\left(v^*, \tau_j, \frac{2\pi}{\omega_0}\right), \Omega_{\xi,2\pi/\omega_0}\right) - \deg_B\left(\mathcal{H}^+\left(v^*, \tau_j, \frac{2\pi}{\omega_0}\right), \Omega_{\xi,2\pi/\omega_0}\right)\\ &= -1.\end{aligned}$$

Consequently, we have

$$\sum_{\left(v^*,\tau_j,2\pi/\omega_0\right) \in D(v^*,\tau,s) \cap N(F)} \gamma(v^*,\tau,s) < 0. \tag{19}$$

Besides, $D(v^*, \tau, s)$ is nonempty.

From the theorem 3.3 in Wu,[25] we know that $D\left(v^*, \tau_j, \frac{2\pi}{\omega_0}\right)$ is unbounded. The proof is completed. □

Lemma 3.2. *All the positive periodic solutions of system (4) are uniformly bounded.*

Proof. Let $(x(t), N(t))$ be a positive nonconstant periodic solution of system (4). Set

$$M_1 = \max\{x(t)|t>0\} = x(\eta_1), \quad M_2 = \max\{N(t)|t>0\} = N(\eta_2),$$
$$m_1 = \min\{x(t)|t>0\} = x(\xi_1), \quad m_2 = \min\{N(t)|t>0\} = N(\xi_2).$$

Since $N(t) > 0$ for all $t > 0$, we have

$$0 = r(1-M_1^3) - \frac{kN(\eta_1)}{1+N(\eta_1)} \leq r(1-M_1^3),$$
$$0 = r(1-m_1^3) - \frac{kN(\xi_1)}{1+N(\xi_1)} \geq r(1-m_1^3) - k.$$

Then, the following is easy to obtain:

$$\max\left\{0, \left(1-\frac{k}{r}\right)^{1/3}\right\} \leq m_1 \leq M_1 \leq 1, \tag{20}$$

Note that

$$0 = \rho x^2(\eta_2-\tau)N(\eta_2-\tau) - dM_2^2 \leq \rho M_1^2 N(\eta_2-\tau) - dM_2^2,$$
$$0 = \rho x^2(\xi_2-\tau)N(\xi_2-\tau) - dm_2^2 \geq \rho m_1^2 N(\xi_2-\tau) - dm_2^2.$$

A direct calculation yields

$$\frac{\rho m_1^2}{d} \leq m_2 \leq M_2 \leq \frac{\rho M_1^2}{d}. \tag{21}$$

The proof is completed. □

Lemma 3.3. *The system (4) has no τ − periodic solution under the assumption*

$$(H_2)\ \rho \leq 3r.$$

Proof. Let $(x(t), N(t))$ be a nonconstant periodic solution to (4) with period τ. Then $(x(t), N(t))$ also is a nonconstant periodic solution for the following ODE system:

$$\begin{cases} \dot{x}(t) = r[1 - x^3(t)] - \dfrac{kN(t)}{1 + N(t)}, \\ \dot{N}(t) = \rho x^2(t)N(t) - dN^2(t). \end{cases} \tag{22}$$

Let $(f(x, N), g(x, N))$ be the vector filed of (22); then for all $(x, N) \in Int(\mathbb{R}_+) \times \mathbb{R}_+$, we have

$$\frac{\partial f}{\partial x} + \frac{\partial g}{\partial N} = (\rho - 3r)x^2 - 2dN. \tag{23}$$

Under the condition (H_2), we have $\frac{\partial f}{\partial x} + \frac{\partial g}{\partial N} < 0$. By the classical Bendixson criterion,[28] we see that the system (22) has no nonconstant periodic solutions lying entirely on $Int(\mathbb{R}_+) \times \mathbb{R}_+$. □

Proposition 1. *Suppose (H_2) is true, then system (4) has no periodic solutions.*

Theorem 3.1. *If (H_1) and (H_2) hold, then system (4) has at least j positive periodic solutions when $\tau > \tau_j$, $j = 1, 2, \ldots$ with τ_j defined in (14).*

Proof. According to the discussion in the beginning of this section, we know that $\left(v^*, \tau_j, \frac{2\pi}{\omega_0}\right)$ are isolate centers. Then $D\left(v^*, \tau_j, \frac{2\pi}{\omega_0}\right)$ is unbounded following Lemma 3.1. Meanwhile, Lemma 3.2 suggests that the projection of $D\left(v^*, \tau_j, \frac{2\pi}{\omega_0}\right)$ onto v-space is bounded. From Proposition 1, one knows the projection of $D\left(v^*, \tau_j, \frac{2\pi}{\omega_0}\right)$ onto τ-space is bounded below.

The definition of τ_j in (14) shows that $2\pi < \tau_j\omega_0 < (2j + 1)\pi$ for $j \geq 1$; then

$$\frac{\tau_j}{j+1} < \frac{2\pi}{\omega_0} < \tau_j. \tag{24}$$

It follows from Lemma 3.3 that if $(v, \tau, s) \in D\left(v^*, \tau_j, \frac{2\pi}{\omega_0}\right)$, then $\frac{\tau}{j+1} < s < \tau$. Thus, the projection of $D\left(v^*, \tau_j, \frac{2\pi}{\omega_0}\right)$ onto the τ-space has to be unbounded so that $D\left(v^*, \tau_j, \frac{2\pi}{\omega_0}\right)$ can be unbounded. This implies that the projection of $D\left(v^*, \tau_j, \frac{2\pi}{\omega_0}\right)$ onto the τ-space covers $[\tau_j, \infty)$. Thus, for each $\tau > \tau_j$, system (4) has j positive nonconstant periodic solutions. The proof is completed. □

Remark 3.1. Since $0 < \omega_0\tau_0 < 2\pi$, we have $\tau_0 < \frac{2\pi}{\omega_0} < \infty$. It has been known that the projection of $D\left(v^*, \tau_j, \frac{2\pi}{\omega_0}\right)$ onto the v-space is bounded. If we further have that the periods of periodic solutions bifurcating from (E_*, τ_0) is bounded, then the unboundedness of $D\left(v^*, \tau_j, \frac{2\pi}{\omega_0}\right)$ leads to that the projection of $D\left(v^*, \tau_j, \frac{2\pi}{\omega_0}\right)$ onto the τ-space is unbounded. Therefore, under conditions (H_1) and (H_2), system (4) has at least $j + 1$ positive periodic solutions for $\tau > \tau_j$, $j = 0, 1, 2, \ldots$. If the the periods of periodic solutions bifurcating from (E_*, τ_0) are unbounded, then the projection of $D\left(v^*, \tau_j, \frac{2\pi}{\omega_0}\right)$ onto the τ-space may not cover $[\tau_0, \infty)$.

4 | NUMERICAL SIMULATIONS

In this section, some numerical simulations are conducted to support the previous theoretical analysis. In particular, we numerically study the ratio of the immune killing rate to tumor volume growth rate, behavior of the Hopf bifurcation,

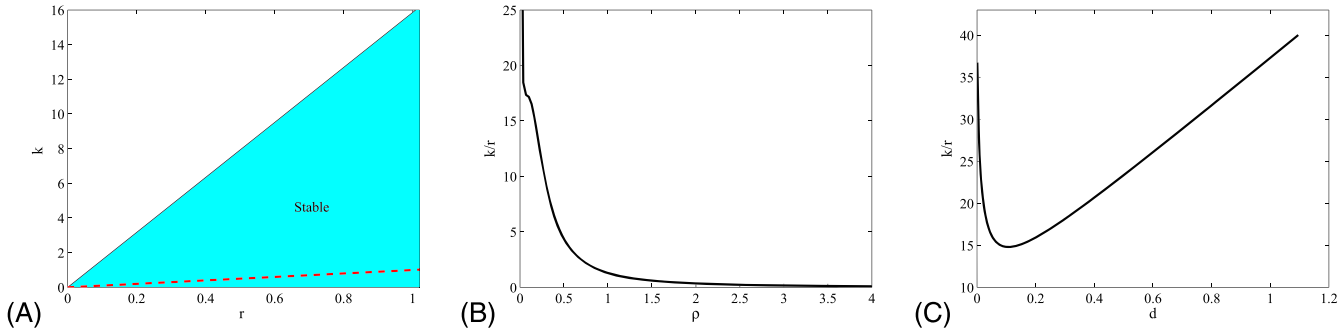

FIGURE 2 (A) The black and red lines are determined by $P(r,k)=0$ and $k=r$, respectively. $P(r,\ k)<0$ above the black line and $P(r,\ k)>0$ below the black line; (B) the effect of ρ on k/r; (C) the effect of d on k/r [Colour figure can be viewed at wileyonlinelibrary.com]

and the effects of other parameters on the first bifurcation value of the immune response time. Considering Table 1, we choose the following parameter values: $T_m=0.5\times10^6$, $r=0.29$, $k=0.9$, $d=0.5$, $\rho=0.24$, and β is chosen by 0.11×10^6.

4.1 | The effect of the killing rate and growth rate

We show the stability change of positive equilibrium driven by the ratio k/r. In Figure 2A, the black line is denoted by $P(r,k)=\frac{\rho r x_*^3}{(d+\rho x_*^2)^2}\Gamma(x_*)$ and the red line stands for $k=r$. It can be checked that the points satisfying $B<D$ are in the region above the black line. The region under the red line must hold $B>D$, where the coexisting state of tumor and CTLs is stable. As the ratio between the growth rate of tumor and the killing rate of CTLs increases and crosses the black line, Theorem 2.4 shows the stability of positive equilibrium may switch and a family of periodic solutions are likely to appear. In fact, oscillations of immune cell number have been observed in some clinical contexts, for example, D'Onofrio.[6] It is clear that there is a critical value of the ratio, below which the positive equilibrium is always locally asymptotically stable and above which periodic solutions may appear.

Understanding how the CTLs recruitment and death rate affect k/r inspires our interest since the ratio determines the competition outcome between CTLs and tumor cells. As illustrated in Figure 2B, CTLs recruitment has a negative effect on the ratio. While the ratio first rapidly decreases then gradually increases as CTLs death rate goes up, as shown in Figure 2C. We have known that it is more possible for the system (4) to undergo the Hopf bifurcation with a large value of k/r. Therefore, when more CTLs die or less CTLs are activated, the stable coexistence of tumor and CTLs will be broken and the volume of the tumor changes in period.

It is known that the size of a tumor indicates the grade malignancy of a tumor; if the tumor volume reaches a certain size, the patient will die. In this study, we have found that the tumor volume may change periodically when the immune response time is long. Once the volume is greater than a specific value, the patient cannot be cured and such oscillations disappear. Suppose that the critical value is $T_0=3\times10^6\mu m^3$. Define *survivaltime* by the first time that the tumor size reaches to T_0. We numerically explore the effect of immune delay on the survival time, which is shown in Figure 3. Observe that shorter response time of the adaptive immune system leads to longer survival time for the patient, and the survival time has a positive minimum value.

4.2 | Numerical simulations of Hopf bifurcation

With the same group of parameter values, some calculations show that the unique positive equilibrium is $(0.3968\times10^6,\ 0.4238\times10^6)$ and the condition $B<D$ is satisfied. Furthermore, we obtain the first Hopf bifurcation value $\tau_0\approx13.4$, and $\omega_0\approx0.07$. Applying Theorem 2.3, E_* is locally asymptotically stable when $\tau\in[0,\ \tau_0)$. When τ passes through τ_0, E_* loses its stability and a family of periodic solutions appear if $\tau>\tau_0$.

Next, we consider the properties of Hopf bifurcations at τ_0. It can be calculated that $c_1(0)\approx-1779.8039-7729.1143$, $\mu_2\approx7.7066$, $\beta_2\approx-3559.6078$, $T_2\approx7537.1536$. Thus, the Hopf bifurcation is forward; the periodic solutions are orbitally asymptotically stable, and their periods increase with time delay. The above results are illustrated in Figures 4 and 5, respectively.

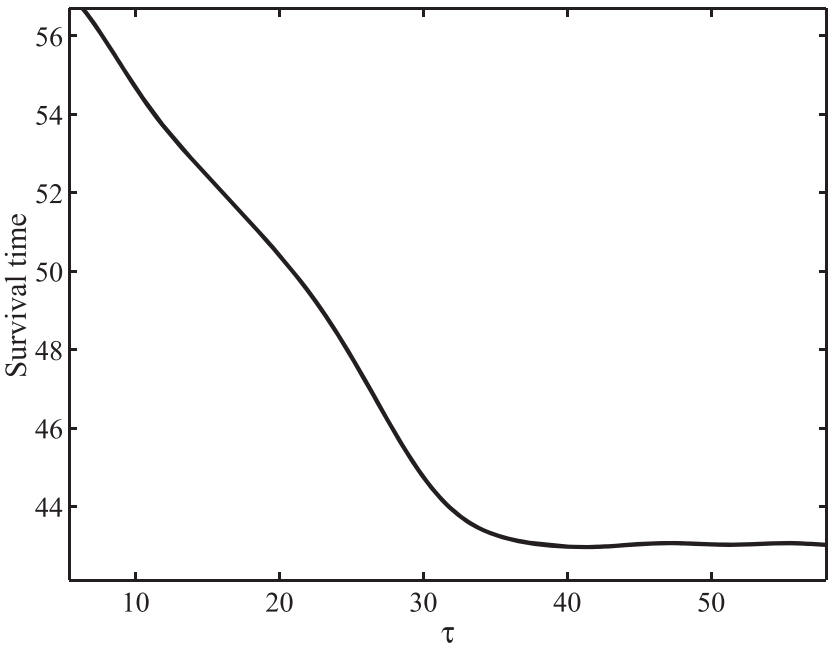

FIGURE 3 Survival time varies with immune delay when initial values are $T(t) = 0.01 \times 10^6, N(t) = 0.82 \times 10^6$

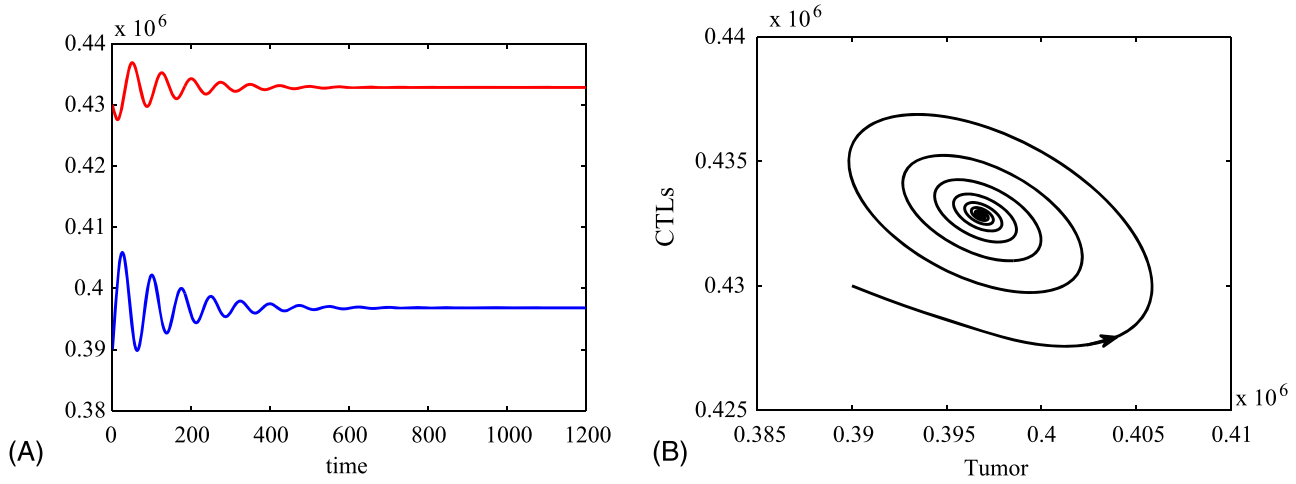

FIGURE 4 The positive equilibrium of system (4) is locally asymptotically stable when $\tau = 9 \in [0, \tau_0)$ (the red curve represents CTL cells and the blue one is tumor cells) [Colour figure can be viewed at wileyonlinelibrary.com]

With the same parameters, we simulate the global behavior of solutions. The Hopf bifurcation diagrams are shown in Figure 6. We see that there is a global continuation of periodic solution bifurcating from Hopf bifurcation when $\tau > \tau_j$, $j \geq 1$.

4.3 | Oscillation behavior affected by other parameters

In this subsection, we numerically explore how other parameters in system (4) affect the oscillation behavior of tumor and CTLs. We first consider how the amount of CTLs affects the first bifurcation value τ_0, which is shown in Figure 7A. This suggests that the oscillation phenomenon of tumor and CTLs is hard to appear when more CTL cells die. The periodic change is easier to occur as the recruitment rate increases that means more immune cells are recruited to the cancer site, as shown in Figure 7B.

Frascoli et al[10] and the assumption (H_1) in this paper both point out that the ratio k/r mostly reflects on the tumor-CTLs interaction dynamics. When other parameters remain unaltered, it can be found that the value of τ_0 is large if tumor growth is fast, which is shown in Figure 8A. In Figure 8B, we can see the change of τ_0 affected by the CTL killing action.

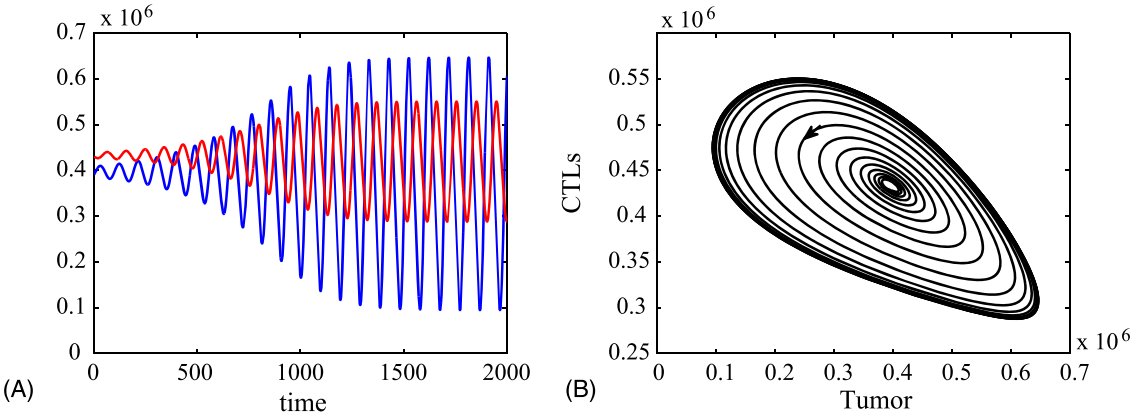

FIGURE 5 When $\tau = 17 > \tau_0$, there is a stable periodic solution bifurcating from the positive equilibrium (the red curve represents CTL cells and the blue one is tumor cells) [Colour figure can be viewed at wileyonlinelibrary.com]

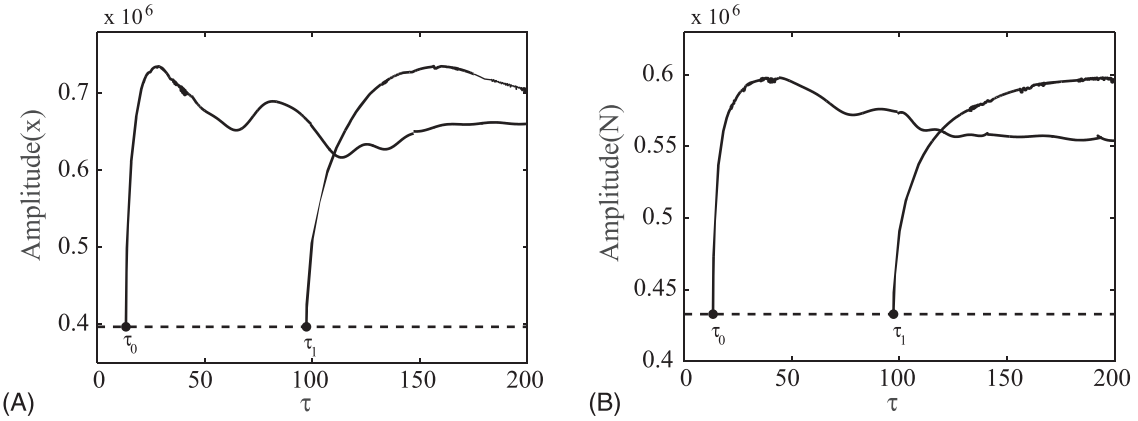

FIGURE 6 The amplitudes of the first two branches of periodic solutions with the initial value (0.3968×10^6, 0.4328×10^6)

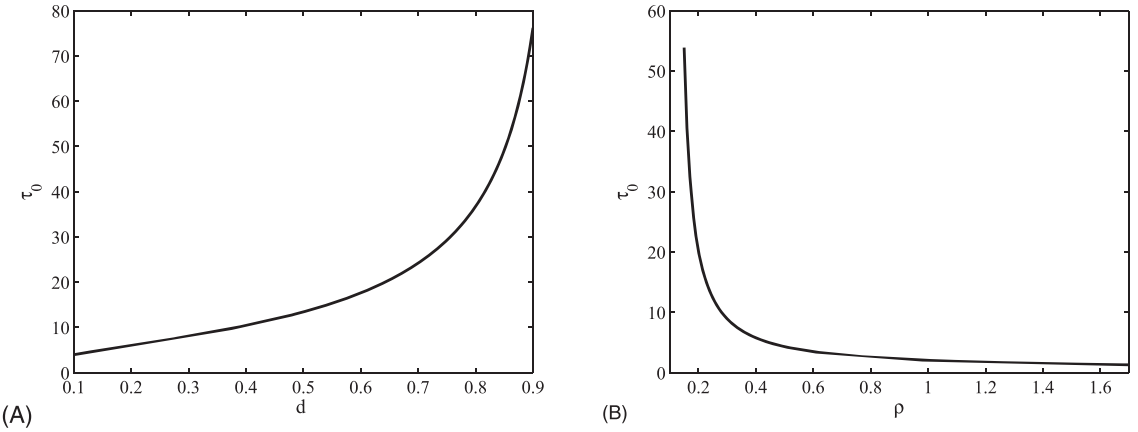

FIGURE 7 (A) The variation of τ_0 with CTL death rate d. (B) The variation of τ_0 with CTL recruitment rate ρ

The joint effect of growth rate and killing rate is presented in Figure 9. We claim that a large killing rate of CTLs and a small growth rate of tumor are favorable for the periodic interacting fashion between tumor and immune system.

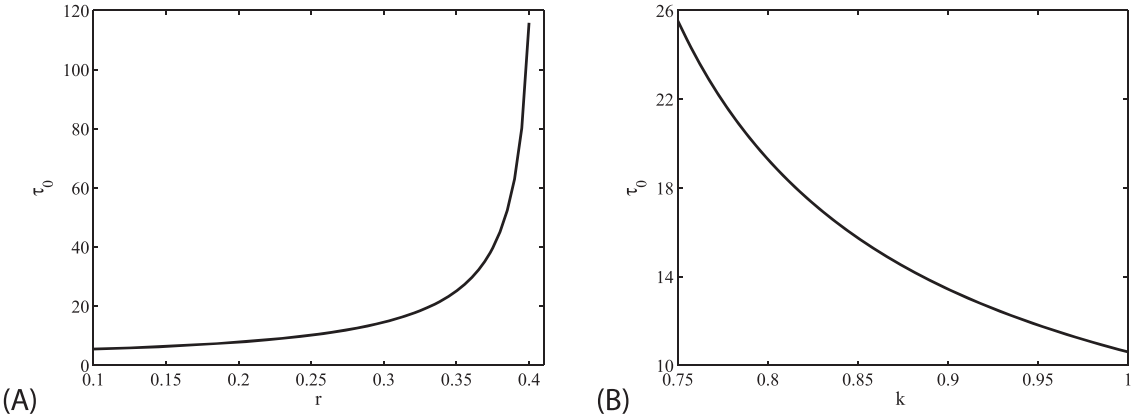

FIGURE 8 (A) Numerical simulation of τ_0 for varying growth rate r. (B) Numerical simulation of τ_0 for varying killing rate k

FIGURE 9 Numerical simulation of τ_0 affected by k and r together [Colour figure can be viewed at wileyonlinelibrary.com]

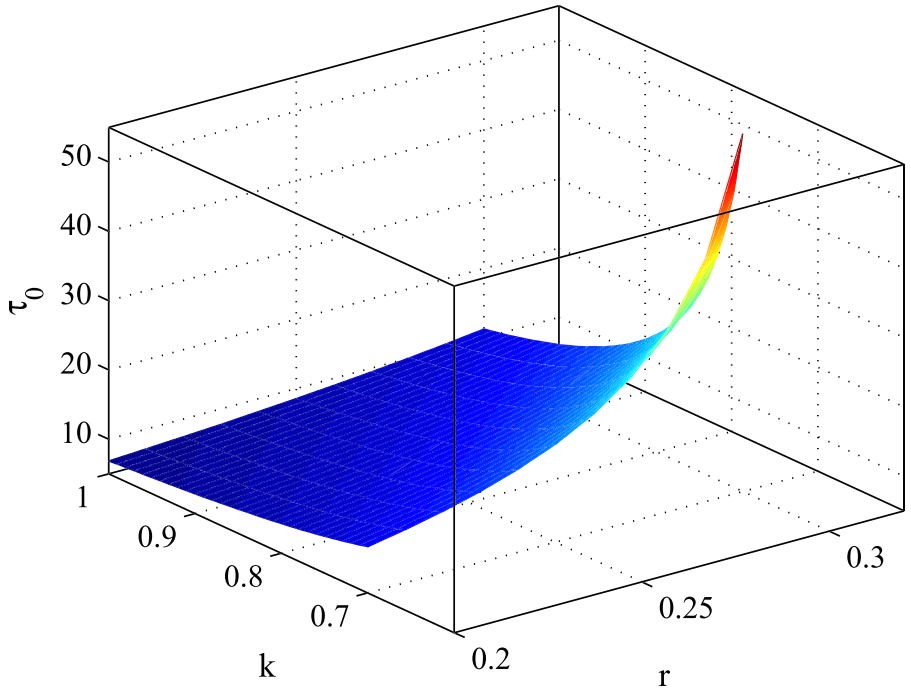

5 | CONCLUSION

In this work, a two-dimensional tumor-immune model with the time delay of the adaptive immune response is studied from the point of view of bifurcation analysis. The avascular growth of a spherical solid tumor is achieved by the proliferating layer cells which is restricted by nutrient supply; thus, the tumor has a finite final size. However, we find the immune-free equilibrium is unstable. Inspired by the fact that dead cells form the necrotic core inside the tumor, we propose the surface growth idea. If the immune system can recognize and attack the tumor in this phase, then it is possible to control the growth of a tumor. We assume the immune response only occurs on the surface of a tumor, so the response function includes the tumor surface area.

For model (4), we confirm that there is a unique coexistence equilibrium and its dynamical behavior closely depends on the ratio of the immune killing rate to tumor volume growth rate. The positive equilibrium is always locally asymptotically stable when the ratio is smaller than a critical value; otherwise there may be oscillation behavior. The adaptive immune response time delay significantly impacts the stability of the positive equilibrium, which drives the system to undergo Hopf bifurcations under certain conditions. We obtain explicit formulas to determine bifurcation direction and stability of bifurcating periodical solutions. We show the global existence of Hopf bifurcating solutions.

Numerically, we find that a shorter immune response time leads to a longer patient survival time and the period and amplitude of a stable periodic solution increase with the immune response time. When CTL recruitment rate and death rate vary, we show how the ratio of the immune killing rate to tumor volume growth rate and the first bifurcation value of the immune response time change numerically, which yields further insights to the tumor-immune dynamics.

It is known that the innate immune system serves as a first defense line. The innate immune system may have different effect on tumor growth.[29] We only consider the adaptive immune response mediated by CTLs in this work. It is necessary to incorporate the innate immune response into modeling of tumor-immune interaction in order to achieve a complete understanding. We plan to consider both innate immune response and adaptive immune response in our future study.

ACKNOWLEDGEMENTS

The authors would like to express their thanks to the referees for their valuable suggestions. HZ, BN, and YXG acknowledge the supports from the Foundation for Innovation at HIT (WH). JPT acknowledges the supports from the National Institutes of Health (U54CA132383) and National Science Foundation of US (DMS-1446139).

CONFLICT OF INTERESTS

The authors declare that they have no conflict of interest.

ORCID

Ben Niu https://orcid.org/0000-0002-7488-9143

REFERENCES

1. Wang W, Epler JE, Salazar LG, Riddell SR. Recognition of breast cancer cells by $CD8_+$ cytotoxic T-cell clones specific for NY-BR-1. *Cancer Res*. 2006;66:6826-6833.
2. Kaufman HL, Kohlhapp FJ, Zloza A. Oncolytic viruses: a new class of immunotherapy drugs. *Nat Rev Drug Discov*. 2015;14:642-662.
3. Byrne HM, Alarcon A, Owen MR, Webb SD, Maini P. Modeling aspects of cancer dynamics: a review. *Philos Trans R Soc Lons Ser A Math Phys Eng Sci*. 2006;364:1563-1578.
4. Li F, Ma W. Dynamics analysis of an HTLV-1 infection model with mitotic division of actively infected cells and delayed CTL immune response. *Math Meth Appl Sci*. 2018;41:3000-3017.
5. Nagy JD. The ecology and evolutionary biology of cancer: a review of mathematical model of necrosis and tumour cell diversity. *Math Biosci Eng*. 2017;2:381-418.
6. D'Onofrio A. A general framework for modeling tumor-immune system competition and immunotherapy: mathematical analysis and biomedical inferences. *Phys D*. 2005;208:220-235.
7. Adam JA, Bellomo N. *A Survey of Models for Tumor-Immune System Dynamics*. Boston: Birkhäuser; 1997.
8. Eftimie R, Bramson JL, Earn DJD. Interaction between the immune system and cancer: a brief review of non-spatial mathematical models. *Bull Math Biol*. 2011;73:2-32.
9. Kuznetsov VA, Makalkin IA, Taylor MA, Perelson A. Nonlinear dynamics of immunogenic tumors: parameter estimation and global bifurcation analysis. *Bull Math Biol*. 1994;56:295-312.
10. Frascoli F, Kim PS, Hughes BD, Landman K. A dynamical model of tumour immunotherapy. *Math Biosci*. 2014;253:50-62.
11. Nestle FO, Tonel G, Farkas A. Cancer vaccines: the next generation of tools to monitor the anticancer immune response. *PLoS Medici*. 2005;2:em339.
12. Kansal AR, Torquato S, Harsh Iv GR, Chiocca E. Simulated brian tumor growth dynamics using a three-dimensional cellular automaton. *J Theoret Biol*. 2000;203:367-382.
13. Dranoff G. Cytokines in cancer pathogenesis and cancer therapy. *Nat Rev Cancer*. 2004;4:11-22.
14. Bi P, Ruan S, Zhang X. Periodic and chaotic oscillations in a tumor and immune system interaction model with three delays. *Chaos*. 2014;24:288-299.
15. Villasana M, Radunskaya A. A delay differential equation model for tumor growth. *J Math Biol*. 2003;47:270-294.
16. Singh HK, Pandey DN. Stability analysis of a fractional-order delay dynamical model on oncolytic virotherapy. *Math Meth Appl Sci*. 2021;44:1377-1393.
17. Kaslik E, Neamtu M. Hopf bifurcation analysis for the hypothalamic-pituitary-adrenal axis model with memory. *Math Med Biol*. 2018;35:49-78.
18. Barza PA. Predator-prey dynamics with square root functional responses. *Nonlinear Anal Real World Appl*. 2012;13:1837-1843.
19. Chattopadhyay J, Chatterjee S, Venturino E. Patchy agglomeration as a transition from monospecies to recurrent plankton blooms. *J Theoret Biol*. 2008;253:289-295.
20. Friedman A, Tian JJP, Fulci G, Chiocca EA, Wang J. Glioma virotherapy: the effects of innate immune suppression and increased viral replication capacity. *Cancer Res*. 2006;66:2314-2319.

21. Hassard BD, Kazarinoff ND, Wan YH. *Theory and application of Hopf bifurcation*. Cambridge-New York: Cambridge University Press; 1981.
22. Faria T. Normal forms for retarded functional differential equations with parameters and applications to Hopf bifurcation. *J Differ Equ*. 1995;122:181-200.
23. Adak D, Bairagi N. Bifurcation analysis of a multidelayed HIV model in presence of immune response and understanding of in-host viral dynamics. *Math Meth Appl Sci*. 2019;42:4256-4272.
24. Wei J. Bifurcation analysis in a scalar delay differential equation. *Nonlinearity*. 2007;20:2483-2498.
25. Wu J. Symmetric functional differential equations and neural networks with memory. *Trans Amer Math Soc*. 1998;350:4799-4838.
26. Hale JK, Lunel SV. *Introduction to Functional Differential Equations*. New York: Springer; 1993.
27. Ruan S, Wei J. On the zeros of transcendental functions with application to stability of delay differential equation with two delays. *Dyn Contin Discrete Impuls Syst Ser A*. 2003;10:863-874.
28. Wiggins S. *Introduction to Applied Nonlinear Dynamical Systems and Chaos*. New York: Springer; 2003.
29. Timalsina A, Tian JJP, Wang J. Mathematical and computational modeling for tumor virotherapy with mediated immunity. *Bull Math Biol*. 2017;79:1736-1758.

How to cite this article: Zhang H, Tian JP, Niu B, Guo Y. Mathematical modeling of tumor surface growth with necrotic kernels. *Math Meth Appl Sci*. 2021;1-19. https://doi.org/10.1002/mma.7571

APPENDIX A

In this section, we choose τ as a bifurcating parameter and derive the explicit formulas determining the properties of Hopf bifurcation under the assumption (H_1). The techniques to be used are normal form method and the centre manifold theory presented in Hassard et al[21] and Faria.[22]

Without loss of generality, write $\tau = \tilde{\tau} + \mu$; then $\mu = 0$ is a Hopf bifurcation point for system (4). Let $x_1(t) = x(t\tau) - x_*$, $x_2(t) = N(t\tau) - N_*$; system (4) becomes

$$\begin{cases} \dot{x}_1(t) = (\tilde{\tau}+\mu)\left[r(1-(x_1(t)+x_*)^3) - \dfrac{k(x_2(t)+N_*)}{1+x_2(t)+N_*}\right], \\ \dot{x}_2(t) = (\tilde{\tau}+\mu)\left[\rho(x_1(t-1)+x_*)^2(x_2(t-1)+N_*) - d(x_2(t)+N_*)^2\right]. \end{cases} \tag{A1}$$

For $\varphi = (\varphi_1, \varphi_2)^T \in C([-1,0], Int(\mathbb{R}_+)\times\mathbb{R}_+)$, let

$$L_\mu\varphi = (\tilde{\tau}+\mu)B_1\varphi(0) + (\tilde{\tau}+\mu)B_2\varphi(-1),$$

with $B_1 = \begin{pmatrix} -3rx_*^2 & \frac{-k}{(1+N_*)^2} \\ 0 & -2dN_* \end{pmatrix}$, $B_2 = \begin{pmatrix} 0 & 0 \\ -2\rho x_* N_* & -\rho x_*^2 \end{pmatrix}$. And

$$f(\mu,\varphi) = (\tilde{\tau}+\mu)\begin{pmatrix} \frac{k\varphi_2^2(0)}{(1+N_*)^3} - \frac{k\varphi_2^3(0)}{(1+N_*)^4} - 3rx_*\varphi_1^2(0) - r\varphi_1^3(0) + O(4) \\ \rho\varphi_1^2(-1)\varphi_2(-1) + \rho N_*\varphi_1^2(-1) - d\varphi_2^2(0) + 2\rho x_*\varphi_1(-1)\varphi_2(-1) \end{pmatrix}. \tag{A2}$$

By the Riesz representation theorem, there is a function $\eta(\cdot,\mu) : [-1,0] \to Int(\mathbb{R}_+)\times\mathbb{R}_+$ of bounded variation, such that

$$L_\mu\varphi = \int_{-1}^{0} \mathrm{d}\eta(\theta,\mu)\varphi(\theta), \ for\, \varphi \in C([-1,0], Int(\mathbb{R}_+)\times\mathbb{R}_+).$$

In fact, $\eta(\cdot,\mu)$ can be taken as

$$\eta(\mu,\theta) = \begin{cases} (\tilde{\tau}+\mu)B_1, & \theta = 0, \\ 0 & \theta \in (-1,0), \\ -(\tilde{\tau}+\mu)B_2, & \theta = -1, \end{cases}$$

For $\varphi \in C^1([-1,0], Int(\mathbb{R}_+)\times\mathbb{R}_+)$, define

$$A(\mu)\varphi(\theta)=\begin{cases}\frac{\mathrm{d}\varphi(\theta)}{\mathrm{d}\theta}, & \theta\in[-1,0),\\ \int_{-1}^{0}\mathrm{d}\eta(\mu,\theta)\varphi(\theta), & \theta=0,\end{cases}\quad R(\mu)\varphi(\theta)=\begin{cases}0, & \theta\in[-1,0),\\ f(\mu,\varphi), & \theta=0.\end{cases}$$

Then, system (4) is equivalent to the following abstract form:

$$\dot{x}_t = A(\mu)x_t + R(\mu)x_t. \tag{A3}$$

with $x=(x_1,x_2)^T$, $x_t(\theta)=x(t+\theta)$, $\theta\in[-1,0]$. For $\psi\in C^1([0,1], Int(\mathbb{R}_+)\times\mathbb{R}_+)$, denote the adjoint operator of $A(\mu)$ by

$$A^*(\mu)\psi(s)=\begin{cases}-\dfrac{\mathrm{d}\psi(s)}{\mathrm{d}s}, & s\in(0,1],\\ \displaystyle\int_{-1}^{0}\psi(-t)\mathrm{d}\eta(t,s), & s=0.\end{cases}$$

The discussion at the beginning of Section 2 implies that $\pm i\tilde{\tau}\omega_0$ are eigenvalues of $A(0)$ and they are also eigenvalues of $A^*(0)$. Let $q(\theta)=(1,P)^Te^{i\omega_0\tilde{\tau}\theta}$, $q^*(s)=E(Q,1)e^{i\omega_0\tilde{\tau}s}$ be the corresponding eigenvectors of $A(0)$ and $A^*(0)$, respectively. Then, using the following bilinear form

$$\langle\psi,\varphi\rangle=\bar{\psi}(0)\varphi(0)-\int_{-1}^{0}\int_{\xi=0}^{\theta}\bar{\psi}(\xi-\theta)\mathrm{d}\eta(\theta)\varphi(\xi)\mathrm{d}\xi,$$

with $\varphi\in C^1([-1,0], Int(\mathbb{R}_+)\times\mathbb{R}_+)$, $\psi\in C^1([1,0], Int(\mathbb{R}_+)\times\mathbb{R}_+)$ and $\eta(\theta)=\eta(\theta,0)$, we have

$$P=-\frac{(3rx_*^2+i\omega_0)(1+N_*)^2}{k},\ Q=\frac{(i\omega_0-2dN_*+\rho x_*^2e^{i\omega_0\tilde{\tau}})(1+N_*)^2}{k}.$$
$$E=\left[(Q+\bar{P})+e^{i\omega_0\tilde{\tau}}\tilde{\tau}(2\rho x_*N_*+\rho x_*^2\bar{P})\right]^{-1}.$$

In what follows, we apply the notations in Hassard et al.[21] Based on the center manifold theorem, we set $W(t,\theta)=W(z(t),\bar{z}(t),\theta)$ on the center manifold C_0 with

$$W(z,\bar{z},\theta)=W_{20}(\theta)\frac{z^2}{2}+W_{11}(\theta)z\bar{z}+W_{02}(\theta)\frac{\bar{z}^2}{2}+W_{30}(\theta)\frac{z^3}{6}+\dots.$$

The solution x_t of system (A1) at $\mu=0$ can be written as

$$x_t=2\mathcal{R}e(z(t)q)+W(z(t),\bar{z}(t)),$$

where $z(t)=\langle q*,x_t\rangle$. We further have

$$\begin{aligned}\dot{z}(t)&=i\omega_0\tilde{\tau}z+\bar{q}^*(\theta)f(0,w(z,\bar{z},\theta)+2\mathcal{R}e(zq(\theta)))\\&=i\omega_0\tilde{\tau}z+\bar{q}^*(0)f(0,w(z,\bar{z},0)+2\mathcal{R}e(zq(0)))\\&=i\omega_0\tilde{\tau}z+\bar{q}^*(0)f_0\\&:=i\omega_0\tilde{\tau}z(t)+g(z,\bar{z}),\end{aligned}\tag{A4}$$

where

$$g(z,\bar{z})=g_{20}\frac{z^2}{2}+g_{11}z\bar{z}+g_{02}\frac{\bar{z}^2}{2}+g_{21}\frac{z^2\bar{z}}{2}+\dots.$$

Therefore,

$$
\begin{aligned}
g_{20} &= 2\bar{E}\tilde{\tau}(\bar{Q},1)\begin{pmatrix} \frac{kP^2}{(1+N_*)^3} - 3rx_* \\ \rho N_* e^{-2i\omega_0\tilde{\tau}} - dP^2 + 2\rho x_* P e^{-2i\omega_0\tilde{\tau}} \end{pmatrix}, \\
g_{11} &= \bar{E}\tilde{\tau}(\bar{Q},1)\begin{pmatrix} \frac{2kP\bar{P}}{(1+N_*)^3} - 6rx_* \\ 2\rho N_* - 2dP\bar{P} + 2\rho x_*(P+\bar{P}) \end{pmatrix}, \\
g_{21} &= 2\bar{E}\tilde{\tau}(\bar{Q},1)\begin{pmatrix} m_{11}+m_{12}+m_{13} \\ m_{21}+m_{22}+m_{23}+m_{24} \end{pmatrix},
\end{aligned}
\tag{A5}
$$

where

$$
\begin{aligned}
&m_{11} = \frac{k}{(1+N_*)^3}\left[W_{20}^{(2)}(0)\bar{P} + 2W_{11}^{(2)}(0)P\right], m_{12} = -3rx_*\left[W_{20}^{(1)}(0) + 2W_{11}^{(1)}(0)\right], \\
&m_{13} = -\frac{3kP\bar{P}}{(1+N_*)^4} - 3r, m_{22} = \rho N_*\left[W_{20}^{(1)}(-1)e^{i\omega_0\tilde{\tau}} + 2W_{11}^{(1)}(-1)e^{-i\omega_0\tilde{\tau}}\right], \\
&m_{21} = 2\rho x_*\left[e^{i\omega_0\tilde{\tau}}\left(W_{20}^{(1)}(-1)\bar{P} + W_{20}^{(2)}(-1)\right) + e^{-i\omega_0\tilde{\tau}}\left(W_{11}^{(1)}(-1)P + W_{11}^{(2)}(-1)\right)\right], \\
&m_{23} = -d\left[W_{20}^{(2)}(0)\bar{P} + 2W_{11}^{(2)}(0)P\right], m_{24} = \rho(2P+\bar{P})e^{-i\omega_0\tilde{\tau}}.
\end{aligned}
$$

Note that the value of g_{21} depends on $W_{20}(\theta)$ and $W_{11}(\theta)$; hence, we still need to compute $W_{20}(\theta)$ and $W_{11}(\theta)$. Note that

$$
\begin{aligned}
\dot{W} &= \dot{x}_t - \dot{z}q - \dot{\bar{z}}\bar{q} = \begin{cases} A(0)W - 2\mathcal{R}e(\bar{q}^*(0)f_0 q(\theta)),\ \theta \in [-1,0), \\ A(0)W - 2\mathcal{R}e(\bar{q}^*(0)f_0 q(0)) + f_0,\ \theta = 0, \end{cases} \\
&\overset{\text{def}}{=} A(0)W + H_{20}(\theta)\frac{z^2}{2} + H_{11}(\theta)z\bar{z} + H_{02}(\theta)\frac{\bar{z}^2}{2} + \dots .
\end{aligned}
\tag{A6}
$$

Due to the chain rule

$$
\dot{W} = \frac{\partial W(z,\bar{z})}{\partial z}\dot{z} + \frac{\partial W(z,\bar{z})}{\partial \bar{z}}\dot{\bar{z}},
$$

then

$$
(A(0) - 2i\omega_0\tilde{\tau})W_{20}(\theta) = -H_{20}(\theta),\ A(0)W_{11}(\theta) = -H_{11}(\theta). \tag{A7}
$$

It can be seen that for $\theta \in [-1, 0)$,

$$
\begin{aligned}
H(z,\bar{z},\theta) &= -q^*(0)f_0 q(\theta) - q^*(0)\bar{f}_0\bar{q}(\theta) \\
&= -g(z,\bar{z})q(\theta) - \bar{g}(z,\bar{z})\bar{q}(\theta).
\end{aligned}
$$

This leads to

$$
H_{20}(\theta) = -g_{20}q(\theta) - \bar{g}_{02}\bar{q}(\theta),\ H_{11}(\theta) = -g_{11}q(\theta) - \bar{g}_{11}\bar{q}(\theta),\ \theta \in [-1,0). \tag{A8}
$$

From (A7), we have

$$
\begin{aligned}
W_{20}(\theta) &= \frac{ig_{20}}{\omega_0\tilde{\tau}}q(0)e^{i\omega_0\tilde{\tau}\theta} + \frac{i\bar{g}_{02}}{3\omega_0\tilde{\tau}}q(0)e^{-i\omega_0\tilde{\tau}\theta} + M_1 e^{2i\omega_0\tilde{\tau}\theta}, \\
W_{11}(\theta) &= -\frac{ig_{11}}{\omega_0\tilde{\tau}}q(0)e^{i\omega_0\tilde{\tau}\theta} + \frac{i\bar{g}_{11}}{\omega_0\tilde{\tau}}\bar{q}(0)e^{-i\omega_0\tilde{\tau}\theta} + M_2,
\end{aligned}
\tag{A9}
$$

where M_1 and M_2 are both two-dimensional vectors.

As $\theta = 0$ in (A6) and (A7), together with the definition of $A(0)$, we have

$$
\begin{aligned}
H_{20}(0) &= -g_{20}q(0) - \bar{g}_{02}\bar{q}(0) + \begin{pmatrix} \frac{2kP^2}{(1+N_*)^3} - 6rx_* \\ 2\rho N_* e^{-2i\omega_0\tilde{\tau}} - 2dP^2 + 4\rho x_* P e^{-2i\omega_0\tilde{\tau}} \end{pmatrix}, \\
H_{11}(0) &= -g_{11}q(0) - \bar{g}_{11}\bar{q}(0) + \begin{pmatrix} \frac{2kP\bar{P}}{(1+N_*)^3} - 6rx_* \\ 2\rho N_* - 2dP\bar{P} + 2\rho x_*(P+\bar{P}) \end{pmatrix}.
\end{aligned}
\tag{A10}
$$

It follows that

$$\begin{pmatrix} 2i\omega_0 + 3rx_*^2 & \frac{k}{(1+N_*)^2} \\ -2\rho x_* N_* e^{-2i\omega_0\tilde{\tau}} & 2i\omega_0 - \rho x_*^2 e^{-2i\omega_0\tilde{\tau}} + 2dN_* \end{pmatrix} M_1 = \begin{pmatrix} \frac{2kP^2}{(1+N_*)^3} - 6rx_* \\ 2\rho N_* e^{-2i\omega_0\tilde{\tau}} - 2dP^2 + 4\rho x_* P e^{-2i\omega_0\tilde{\tau}} \end{pmatrix}. \tag{A11}$$

and

$$\begin{pmatrix} 3rx_*^2 & \frac{k}{(1+N_*)^2} \\ -2\rho x_* N_* & -\rho x_*^2 + 2dN_* \end{pmatrix} M_2 = \begin{pmatrix} \frac{2kP\bar{P}}{(1+N_*)^3} - 6rx_* \\ 2\rho N_* - 2dP\bar{P} + 2\rho x_*(P + \bar{P}). \end{pmatrix} \tag{A12}$$

Now $W_{20}(\theta)$ and $W_{11}(\theta)$ could be obtained and g_{21} could be presented explicitly. Consequently, $c_1(0)$ and other quantities could be directly expressed in terms of parameters and delay mentioned in (A1).

$$\begin{aligned} c_1(0) &= \frac{i}{2\omega_0\tilde{\tau}}\left(g_{11}g_{20} - 2|g_{11}|^2 - \frac{|\bar{g}_{20}|^2}{3}\right) + \frac{g_{21}}{2}, \\ \mu_2 &= -\frac{\mathcal{R}e(c_1(0))}{\mathcal{R}e(\lambda_0'(\tilde{\tau}))}, \\ \beta_2 &= 2\mathcal{R}e(c_1(0)), \\ T_2 &= -\frac{\mathcal{I}m(c_1(0)) + \mu_2\mathcal{I}m(\lambda_0'(\tilde{\tau}))}{\omega_0}. \end{aligned} \tag{A13}$$

According to the general Hopf bifurcation theory in Hassard et al,[21] it is known that μ_2 determines the direction of Hopf bifurcation: if $\mu_2 > 0 (\mu_2 < 0)$, then a branch of periodic solutions appear for $\tau > \tilde{\tau} (\tau < \tilde{\tau})$; β_2 determines the stability of the bifurcating periodic solutions: the bifurcating periodic solutions in the center manifold are stable (unstable) if $\beta_2 < 0 (\beta_2 > 0)$; T_2 determines the period: the period increases (decreases) if $T_2 > 0 (T_2 < 0)$.